Available online at www.sciencedirect.com
ScienceDirect
Trans. Nonferrous Met. Soc. China 32(2022) 2557−2568
Transactions of Nonferrous Metals Society of China
www.tnmsc.cn

Microstructure evolution and ductility improvement mechanisms of magnesium alloy in interactive alternating forward extrusion

Hua-qiu DU[1], Feng LI[1,2], Peng-da HUO[1], Yu WANG[1]

1. School of Materials Science and Chemical Engineering, Harbin University of Science and Technology, Harbin 150040, China;
2. Key Laboratory of Advanced Manufacturing and Intelligent Technology, Ministry of Education, Harbin University of Science and Technology, Harbin 150080, China

Received 9 August 2021; accepted 18 January 2022

Abstract: The microstructural evolution and mechanical properties of AZ31 magnesium alloy processed by the interactive alternating forward extrusion at different loading displacements (h=3, 6, 9 mm) were investigated. Optical microscopy (OM) and electron backscatter diffraction (EBSD) were used to analyze the evolution of microstructure, and the mechanical behavior was clarified by tensile tests and scanning electron microscopy (SEM). The results show that continuous dynamic recrystallization (CDRX) and discontinuous dynamic recrystallization (DDRX) can achieve grain refinement jointly in interactive alternating forward extrusion. With the decrease of the loading displacement h, the proportion of recrystallization increases from 23.4% to 66.7%. The fiber texture gradually tilts to the extrusion direction (ED), and the grain orientation randomization of DDRX further weakens the fiber texture intensity. When h=3 mm, the ultimate tensile strength (UTS) is 249.1 MPa and the elongation can reach 29.4%.
Key words: magnesium alloy; alternating extrusion; grain refinement; texture weakening

1 Introduction

Traditional magnesium alloys are mostly produced by the casting process, which has many defects, such as low tensile strength, poor compactness, and low ductility. In comparison, the wrought magnesium alloys have finer and more uniform microstructures, and better comprehensive properties [1−7].

The metals which can easily obtain excellent microstructures are caused by triaxial compressive stress during the extrusion process. Therefore, the extrusion process is especially suitable for the preparation and processing of magnesium alloys [8−10]. FENG et al [11] studied the microstructure evolution and mechanical properties of AZ31 magnesium alloy during semi-solid extrusion (SSE). They found that there is an obvious texture weakening phenomenon in the SSE process. The ductility of magnesium alloy was greatly improved compared with traditional extrusion. PAN et al [12] prepared a kind of AZ31 sheet with high strength and ductility by composite extrusion. The results showed that the elongation of the extruded sheets could increase from 18.5% to 22.5%, and the tensile strength reached 350 MPa. Therefore, the ductility and tensile strength of extruded sheets at room temperature were greatly improved with the formation of the fine and uniform microstructure in the matrix. YANG et al [13] carried out a systematic study on asymmetric extrusion (AE). Compared with traditional extrusion, the elongation was increased to 24.4%. The results showed that a tilted

Corresponding author: Feng LI, Tel: +86-451-86392501, E-mail: fli@hrbust.edu.cn;
Peng-da HUO, Tel: +86-451-86392501, E-mail: hpd0609@163.com
DOI: 10.1016/S1003-6326(22)65965-X

weak basal texture and microstructure refinement were obtained in the AE AZ31 sheet compared with the conventional extrusion (CE) AZ31 sheet. Asymmetric extrusion provided new ideas for the study of high-property magnesium alloys. ZHANG et al [14] used low-speed extrusion to produce AZ31 sheets at different temperatures. They found that low-speed extrusion could effectively refine the grains of magnesium alloys, the average grain size reached 2.7 μm at 623 K, and the tensile strength reached 353 MPa. ZHANG et al [15] adopted a porthole die extrusion to fabricate hollow magnesium profiles, and the method could increase shear deformation in the extrusion process. The results showed that weakening texture intensity had a significant impact on the strength and elongation of the magnesium alloy. The tensile strength of the profile ranged from 290.5 to 296.0 MPa, and its elongation ranged from 20.9% to 22.1%.

In this study, the alternating forward extrusion (AFE) process which is practical and economical was applied to producing the AZ31 bar [16]. AFE as a new extrusion technology was proposed and attracted the attention in the industry. The metal flow behavior has been changed during AFE. Most of the magnesium alloy flows to the die mouth under the action of the punch, and other part flows to the punch below, so the dead zone area is greatly reduced. The billet utilization is significantly improved [17]. Owing to the significant grain refinement and texture weakening effects induced by the AFE process, both the strength and ductility of Mg alloy can be effectively improved [18]. The loading displacement h of the split punch is the key to AFE, which can affect the metal flow and the evolution of the microstructure. This study aims to illuminate the effect of texture and microstructure on mechanical properties at different loading displacements.

2 Experimental

2.1 Principle

A special structure design for punch was adopted in AFE process, and the principle of AFE is presented in Fig. 1. Compared with conventional extrusion, the billet was extruded after continuous shear deformation.

AFE can be divided into progressive and interactive loading methods according to the movement mode of the punch. Compared with the former, the interactive loading method is more conducive to improving the forming efficiency of the extruded product. So, two split punches are alternately loaded during the interactive AFE process. The loading displacement (h) of the single split punch was 3, 6, and 9 mm.

2.2 Materials and methods

The experimental billet was a cylinder with both diameter and height of 40 mm. Commercial extruded feedstock of AZ31 magnesium alloy rod was used as the sample material. The chemical composition is given in Table 1. The extrusion experiment was conducted on a YT32-100 type apparatus. The water-based graphite was used as lubricant. The forming temperature was 623 K. The extrusion speed was 1 mm/s. The extrusion ratio was 8.16.

Samples from the AFE AZ31 bars were machined into cylinders with dimensions of 5 mm in extrusion direction (ED) and 14 mm in transverse

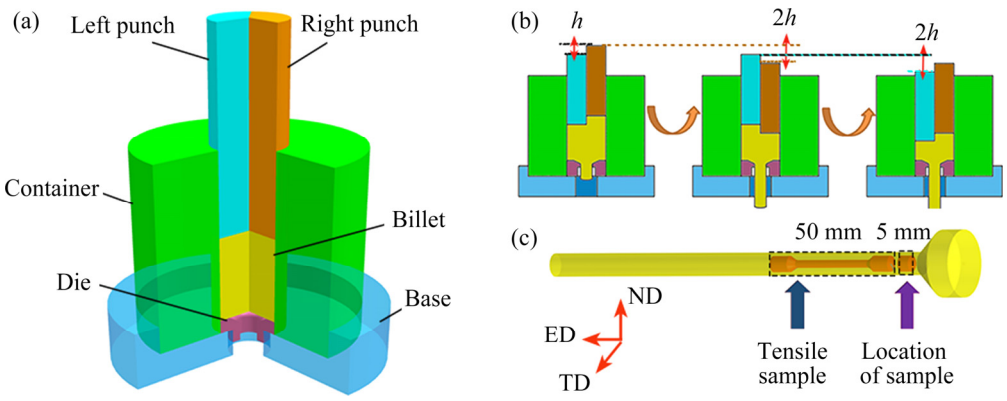

Fig. 1 Principle of interactive alternating forward extrusion: (a) Schematic diagram of principle; (b) Process flow; (c) Sampling location

Table 1 Chemical composition of AZ31 magnesium alloy (wt.%)

Al	Zn	Mn	Fe	Si	Cu	Ni	Mg
3.20	0.86	0.36	0.0018	0.021	0.0022	0.00056	Bal.

direction (TD) to investigate the microstructure and texture evolutions. The sampling location is shown in Fig. 1. Water milling was performed on 80#, 400#, 1500#, 3000#, and 5000# waterproof abrasive paper. The microstructure was observed and analyzed by a LEICA metallographic microscope. After the process of mechanical polishing, electro-polishing was used on the samples. The polishing fluid was a mixed solution of phosphoric acid and alcohol (volume ratio was 3:5). After polishing at 0.3 A for 80 s and then 0.2 A for 70 s, electron backscattered detection (EBSD) of samples was carried out by a Quanta 200F field emission electron microscope (the scanning area was 300 μm × 300 μm, the step size was 1.5 μm, the sample stage was inclined at 70°, and the working distance was 13 mm). Then, the obtained data were analyzed by channel 5 software. A RigakuD/MAX-2500PC X-ray diffractometer was used to measure the grain orientation of samples. The tube voltage was 35 kV. The tube current was 40 mA. The measurement angle range was 20°−80°.

Tensile tests were conducted on an electronic universal testing machine (Instron 5569). The size of the test sample was *d*5 mm × 50 mm. The loading speed was 1 mm/min. An APREO field emission scanning electron microscope was used to observe and analyze the tensile fracture morphology.

3 Results and discussion

3.1 Microstructures

Compared with conventional extrusion, the highly plastically deformed shear zone is created throughout the region between the two punches. Therefore, it is necessary to study the microstructure and properties of extruded products under different loading displacement *h*. The microstructures of the extruded products at different *h* are shown in Fig. 2.

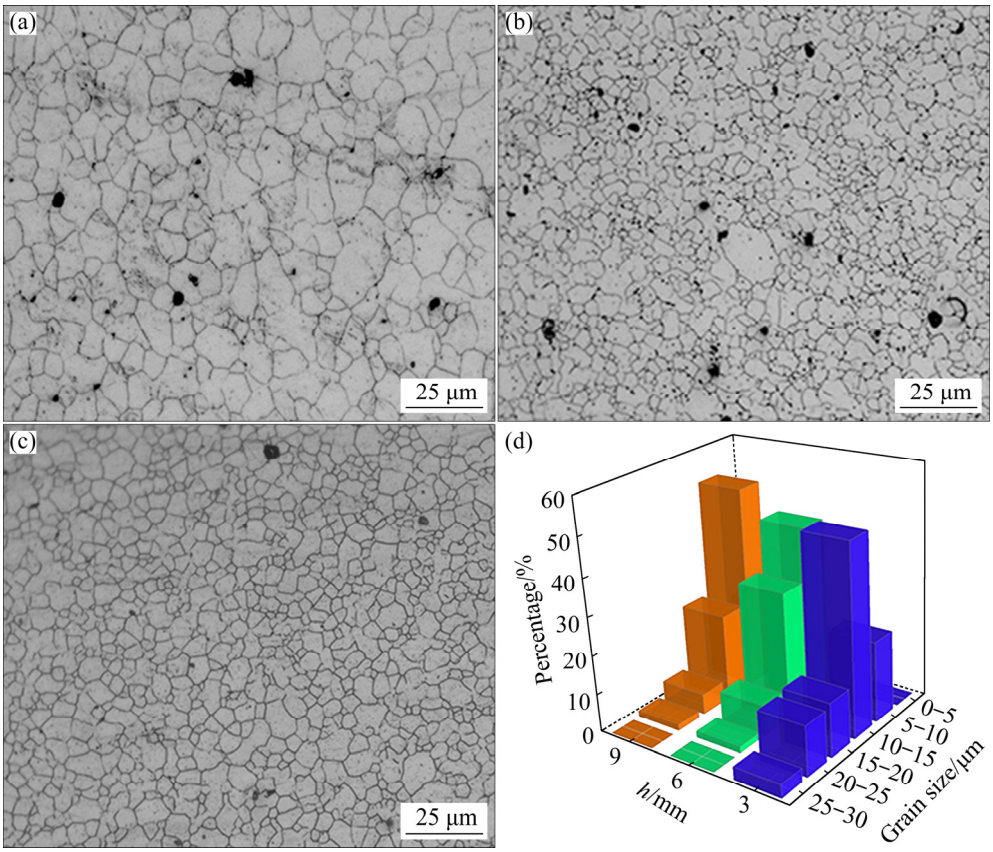

Fig. 2 Comparison of metallographic morphology under different loading displacements: (a) *h*=3 mm; (b) *h*=6 mm; (c) *h*=9 mm; (d) Histogram of grain size statistics

When h=3 mm, the metallographic microstructure of the extruded products is shown in Fig. 2(a). The average grain size is approximately 14 μm. The metallographic microstructure at h=6 mm is shown in Fig. 2(b), some coarse grains are broken into small grains, and some grains are surrounded by fine grains. The average grain size is approximately 11 μm at h=6 mm. The smallest grain size can reach 4.7 μm, and the largest grain size exceeds 25 μm. When h=9 mm, the average grain size is approximately 9.5 μm, as shown in Fig. 2(c). The smallest grain size is 4.06 μm and the maximum grain size is over 30 μm. There is a phenomenon of fine-grain aggregation in some areas. In summary, when h=6 and 9 mm, although the average grain size decreases, the degree of non-uniformity increases significantly.

3.2 Mechanical properties

The tensile test was performed at a tensile strain rate of 1 mm/min. The ultimate tensile strength (UTS) and uniform elongation (E_u) under different conditions are shown in Fig. 3. When h=3 mm, the ultimate tensile strength reaches 249.1 MPa. When h=6 mm, UTS is slightly increased to 257.3 MPa. When h is increased to 9 mm, the UTS reaches 273.4 MPa. Compared with h=3 mm, UTS increases by nearly 9.8% when h=9 mm.

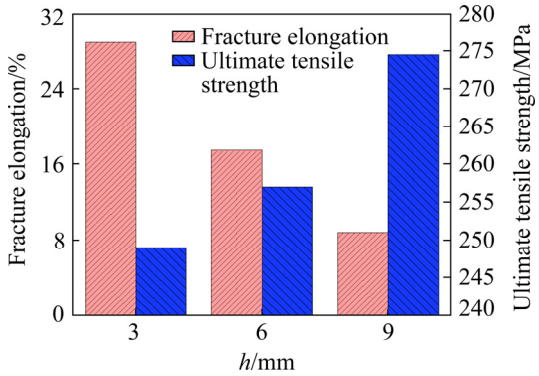

Fig. 3 Comparison of mechanical properties

In addition, although the UTS is improved to some extent at h=9 mm, the E_u is only 8.82%. When h=3 mm, the E_u can reach 29.4% and the UTS is relatively low. Compared with the former, the bar elongation is increased by nearly 2.33 times. In conclusion, the ductility is the best when h=3 mm.

Due to the lack of second phase particles in AZ31 after homogenization, grain boundary strengthening plays a major role in improving tensile strength. A large number of grain boundaries hinder dislocation movement [19]. During the tensile process, due to the uniformity of microstructure at h=6 and 9 mm being poor, stress concentration is generated between the coarse and the fine grains, which causes the fracture of the material in advance. The behavior of brittle fracture can be confirmed by a large number of cleavage steps in the fracture microstructures, as shown in Fig. 4. After a comprehensive comparison, when h=3 mm, although the UTS decreases, the ductility is greatly improved.

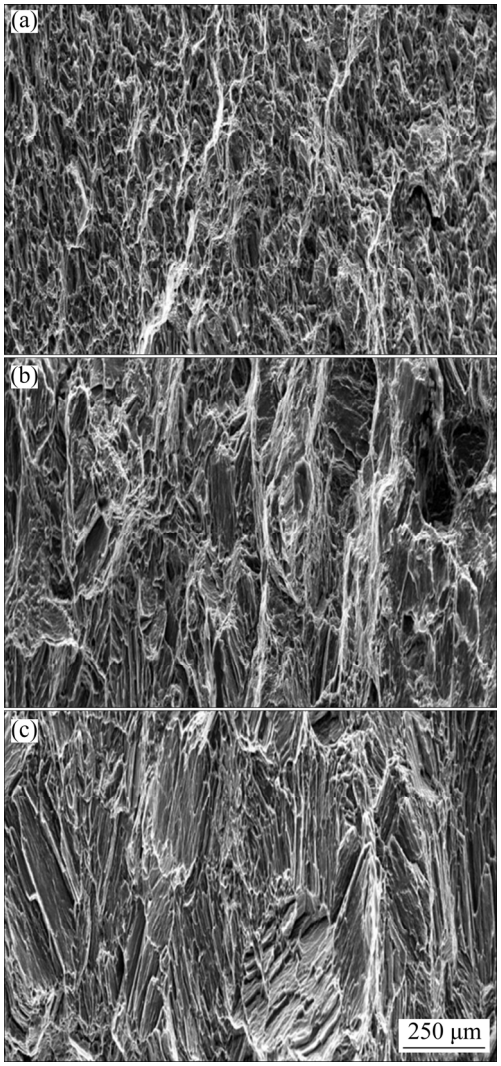

Fig. 4 Comparison of fracture microstructures: (a) h=3 mm; (b) h=6 mm; (c) h=9 mm

The fracture surfaces at different h are shown in Fig. 4. When h=3 mm, many equiaxed dimples are randomly distributed in Fig. 4(a), and there are

almost no cleavage steps. When h=6 mm, as shown in Fig. 4(b), there are cleavage planes and cleavage steps in a local area of the fracture surfaces. When h=9 mm, a predominant feature of the fracture surface is the occurrence of cleavage facets and steps. Compared with the former two, the plastic deformation capacity of the sample is further reduced, and brittle fracture is prone to occur at h=9 mm.

3.3 Dynamic recrystallization behavior

The microstructures including different grain types obtained at different loading displacements are shown in Fig. 5. The white lines in the figure are low-angle grain boundaries (LAGBs, grain boundary misorientation angle θ_{GB}<15°). The black lines are high-angle grain boundaries (HAGBs, θ_{GB}>15°). In Fig. 5, diverse types of grains are marked with different colors. Figure 6 shows the proportion of various grains at loading displacements of 3, 6, and 9 mm.

Figures 5(a) and 6 show that the number of recrystallized grains is the largest at h=3 mm, which can reach 66%. The proportion of substructure grains is 26%, and the deformed grains is 8%. The research shows that the grain orientation randomization of discontinuously dynamic recrystallization (DDRX) weakens the fiber texture [20]. The texture is essentially preferred orientation of grains. DDRX disperses the preferred orientation to a certain extent. The KAM (Kernel average misorientation) in Fig. 5(c) reveals the recrystallization mechanism at h=3 mm. In the magnesium alloy with low stacking fault energy, the

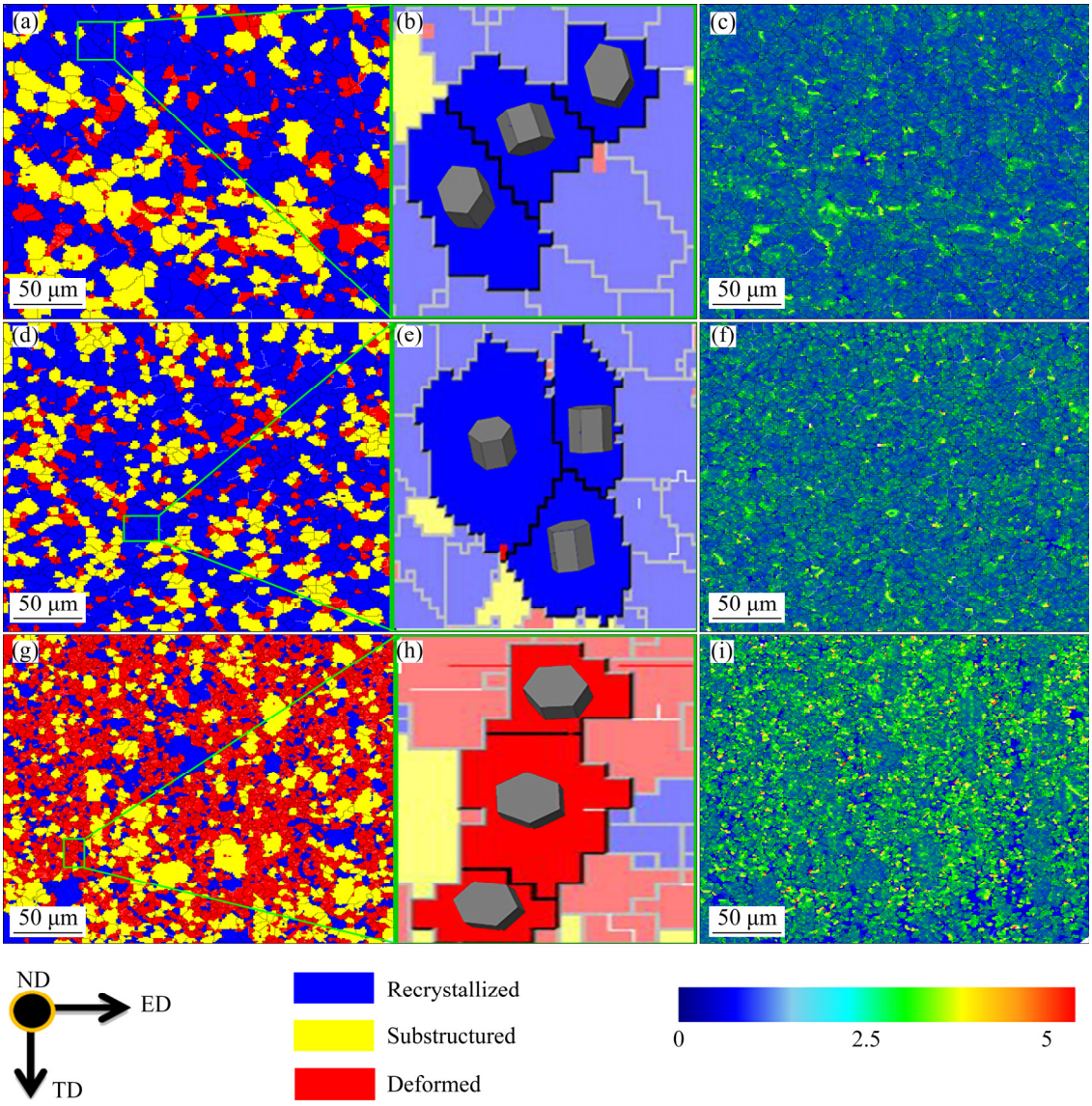

Fig. 5 Grain type distributions (a, b, d, e, g, h) and KAM diagrams (c, f, i): (a−c) h=3 mm; (d−f) 6 mm; (g−i) 9 mm

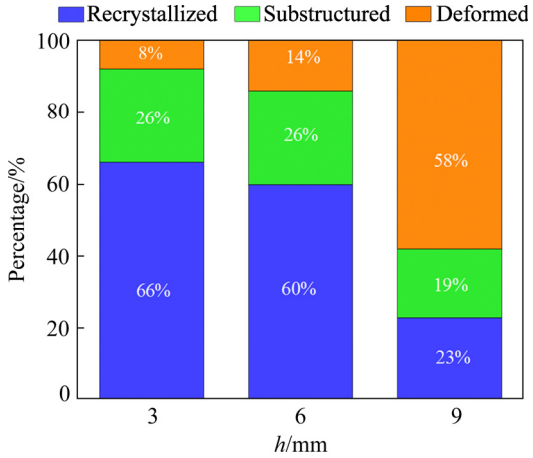

Fig. 6 Percentage of grain types

nucleation of dynamically recrystallized grains is mainly divided into three mechanisms: CDRX (nucleated by sub-grain rotation), DDRX (nucleated by grain boundary bugling), and TDRX (twinning-aided dynamic recrystallization, and nucleated by twinning intersection) [21]. There are two main nucleation mechanisms of dynamic recrystallization: direct nucleation of the original grain boundaries and grain boundary migration (The proportion of original grains gradually decreases, and recrystallization gradually increases) [22]. The formation of a new grain structure in a deformed material by the formation and migration of HAGBs is driven by the stored energy. In KAM, the color of the rainbow gradient shows that the most energy is distributed around the sub-grain boundary [23]. Figures 5(d) and 6 show that when h=6 mm, the proportions of recrystallized grains, sub-grain structures, and deformed grains are 60%, 26% and 14%, respectively. Figure 5(e) shows the orientation of the partially recrystallized grains, and the misorientation angle between the recrystallized grains is low. CDRX is the gradual migration of LAGBs into HAGBs (forming the dynamically recrystallized grains by sub-grain structure) [24,25]. During the CDRX process, the recrystallized grains only rotate slightly based on the parent grains [26]. Figure 5(g) shows that when h=9 mm, the proportion of recrystallized grains is low, and more deformed grains are preserved. Figures 5(g, i) show the orientation of partially deformed grains and the energy density distribution in the KAM. The energy density in KAM is high at h=9 mm, and the sub-grain boundary fails to completely consume energy to recrystallize. Therefore, the proportion of recrystallized grains is low. The stored energy is higher at h=9 mm, and the dislocation pile-up made by the dislocation motion leads to LAGBs evolving into HAGBs as the deformation progresses. At h=9 mm, many deformed grains can be observed, and the average grain size is small. During the plastic deformation process, grain refinement is a process of grain fragmentation or recrystallization nucleation. The recrystallization of many grains is incomplete, and the rotation of grain boundaries and the dislocation climbing do not promote the annihilation of high-density dislocations at the grain boundaries. Therefore, most of the fine grains are identified as deformed grains in EBSD.

Necklace structure composed of dynamically recrystallized grains shown in Fig. 5(a) is formed, which is a sign of DDRX. So, DDRX is the main recrystallization mechanism at h=3 mm.

To further reveal the DRX mechanism under different h, Fig. 7 shows the misorientation angle and the proportion of LAGBs, MAGBs (medium-angle grain boundaries, $3°<\theta_{GB}<15°$), and HAGBs at different h. The growth of grains is affected by the migration of HAGBs [27]. When h=3 mm, the proportion of HAGBs is 57.31%. When h=6 mm and 9 mm, the proportions of HAGBs are 56.58% and 55.37%, respectively. The dynamic recrystallization grains can introduce more HAGBs, and there are more MAGBs but fewer LAGBs at h=6 mm [28]. MAGBs can be seen as an intermediate stage from LAGBs to HAGBs. Increasing the MAGBs can enhance the CDRX. CDRX is a process in that LAGBs continuously accumulate dislocations during deformation, and the accumulated dislocations do not participate in strain hardening. When h=9 mm, mixed crystals are found in Fig. 7(c). The evolution of LAGBs to HAGBs occurs by uniformly increasing the orientation difference of LAGBs at high temperatures. The grains near the initial grain boundaries are formed by rotating or forming micro-shear bands at large strain. The recrystallization nucleation in the DDRX mechanism is mainly related to the HAGBs migration. During the nucleation process of DDRX, in the initial stage of deformation, HAGBs lead to inhomogeneous deformation accompanied by the formation of orientation gradients, which will promote the expansion of HAGBs. Dynamic recrystallization nucleates at the initial grain

boundaries. When h=3 mm, partial grain boundaries bow out, which is a typical feature of DDRX. To make the results clearer, Fig. 8 shows the CDRX and DDRX mechanisms at different h.

3.4 Schmid factor

Figure 9 shows the Schmid factor distribution at different loading displacements. The Schmid factor is also called the orientation factor. The

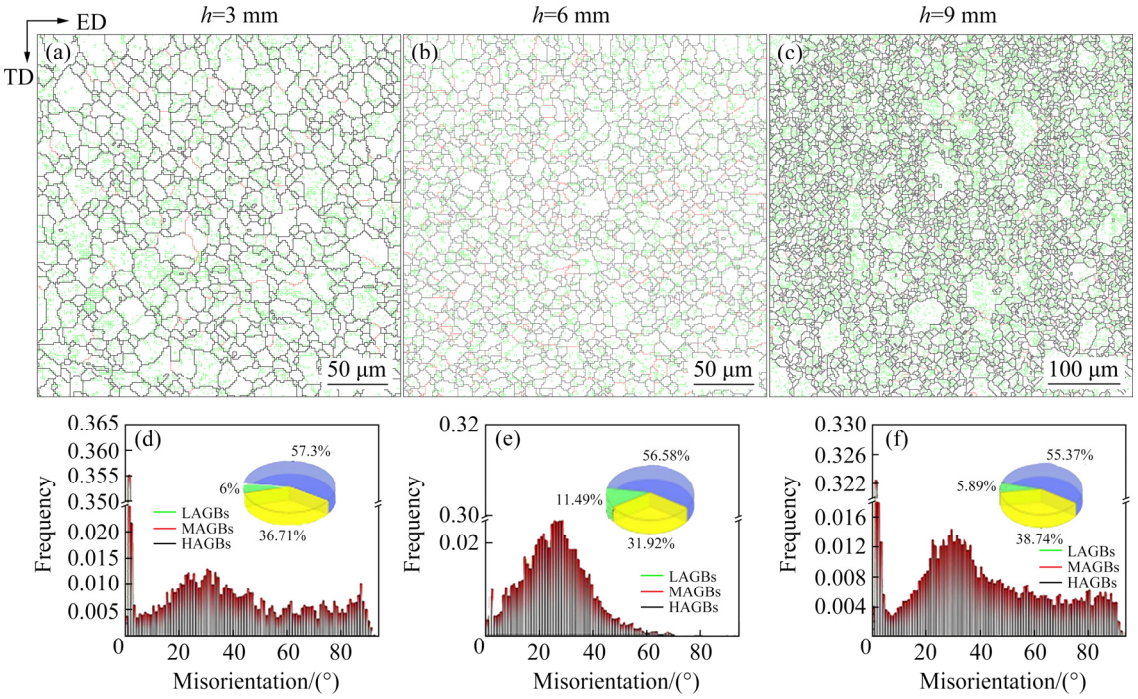

Fig. 7 Contrast of misorientation angle: (a−c) Grain boundary microstructures; (d−f) Grain boundary angle statistics

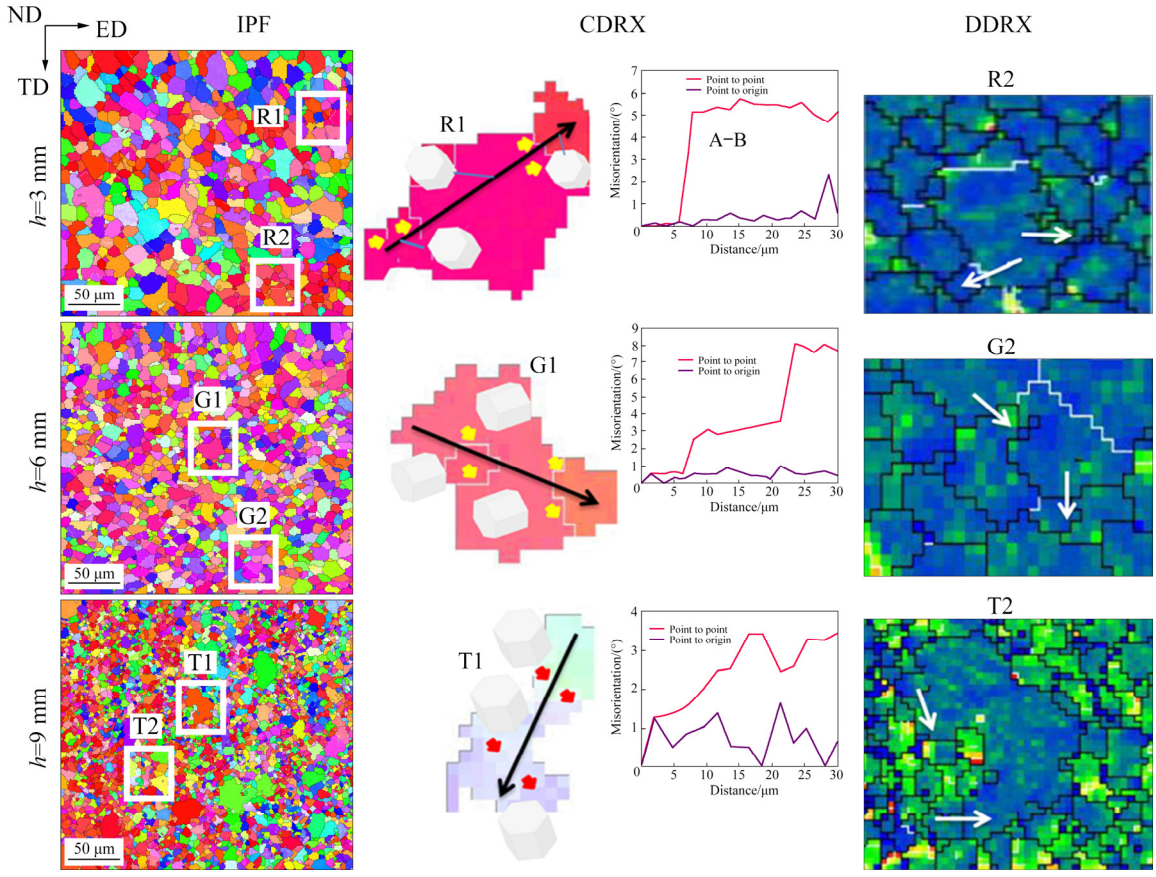

Fig. 8 CDRX and DDRX mechanisms at different h

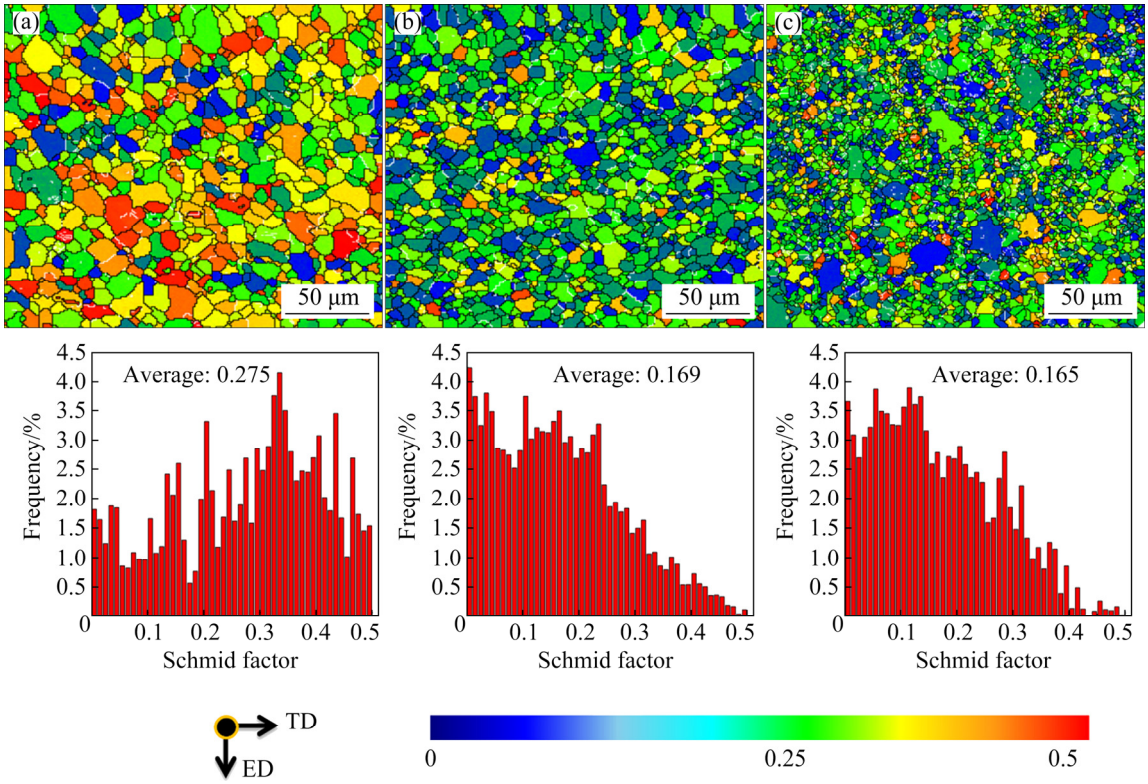

Fig. 9 Comparison of Schmid factor distribution on base plane: (a) h=3 mm; (b) h=6 mm; (c) h=9 mm

different colors in Fig. 9 represent the Schmid factor value of different grains. The color is distributed in a gradient from blue to red, and the Schmid factor also increases accordingly.

The critical resolved shear stress (CRSS) and Schmid factor are the key factors in the deformation of magnesium alloys. A high Schmid factor and low CRSS will promote the activation of the slip system [29]. Figure 9(a) shows the Schmid factor distribution when h=3 mm. The Schmid factor value along the extrusion direction is generally higher, the number of red or orange grains is significantly larger, and there are only a few blue grains. The Schmid factor is closely related to the activation of the slip system [30]. The higher the Schmid factor is, the lower the yield limit of the corresponding single grain [31]. When the angle between the direction of the loading force and the slip direction of the slip plane is 45°, the Schmid factor has a maximum value of 0.5, and basal slip is easily activated at this time, which can provide a better answer to why the ductility of the sample is excellent at h=3 mm [32].

When h=6 mm, the Schmid factor distribution is shown in Fig. 9(b). There are many blue or green grains and a few red grains. The average Schmid factor is 0.169, so it is more difficult to activate the slip systems.

Figure 9(c) shows Schmid factor distribution with h=9 mm. The Schmid factor is the lowest (the average Schmid factor is 0.165).

According to the above results, when h=6 and 9 mm, there are more hard-orientated grains. There are more soft-orientated grains at h=3 mm, and the slip of dislocations on the crystal plane is easier than hard-orientated dislocations [33]. Therefore, as h decreases, the Schmid factor gradually increases.

3.5 Texture analysis

The parameters k and σ_0 in Hall−Petch (H−P) equation can be affected by texture [34]. Because the value of k is affected by the local grain orientation, if the orientation relationship of adjacent grains changes, the value of k can be changed independently. The preferred orientation of grains is particularly important in magnesium alloy because there are fewer slip systems that can be activated at room temperature [35]. Therefore, the mechanical properties of the sample can be affected by texture, and the value of the Schmid factor can be influenced by texture also.

The comparison of the results of X-ray

diffraction tests under different h values is shown in Fig. 10. The texture of the sample can be analyzed by EBSD, but the scanning area of EBSD is small. XRD was used to measure the intensity of diffraction peaks for macrotexture analysis. The intensity of the diffraction peaks depends on the crystal structure, which is formed by stacking crystal planes. According to Fig. 10, different crystal planes have different diffraction peaks. The X-ray diffraction intensities of each crystal plane at h values of 3, 6, and 9 mm mainly contain texture components such as $(10\bar{1}0)$, (0002), and $(1\bar{1}06)$. Due to the differences in h values, the preferred orientation of grains is also different. When h=3 mm, the strongest peak is $(10\bar{1}1)$. When h=6 and 9 mm, the diffraction peaks of $(10\bar{1}0)$ and (0002) are not much different. With increasing h, the orientation of more grains is deflected toward $(10\bar{1}0)$ and (0002). The grain deflection hinders the movement of the dislocations to a certain extent.

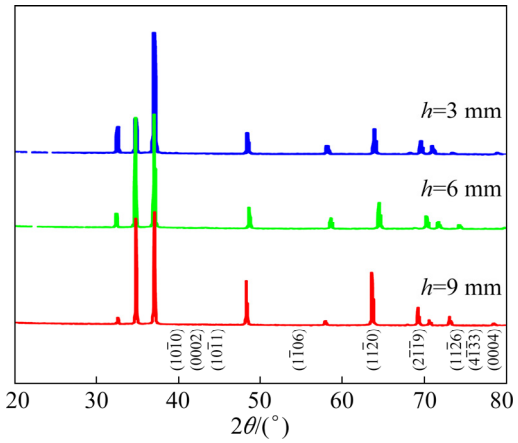

Fig. 10 XRD patterns under different h values

To analyze the evolution of texture with different values of h more intuitively, the pole figure and inverse pole figure are shown in Fig. 11. The texture has a tilt of approximately 34° in the TD and ED directions in Fig. 11(a). The strongest

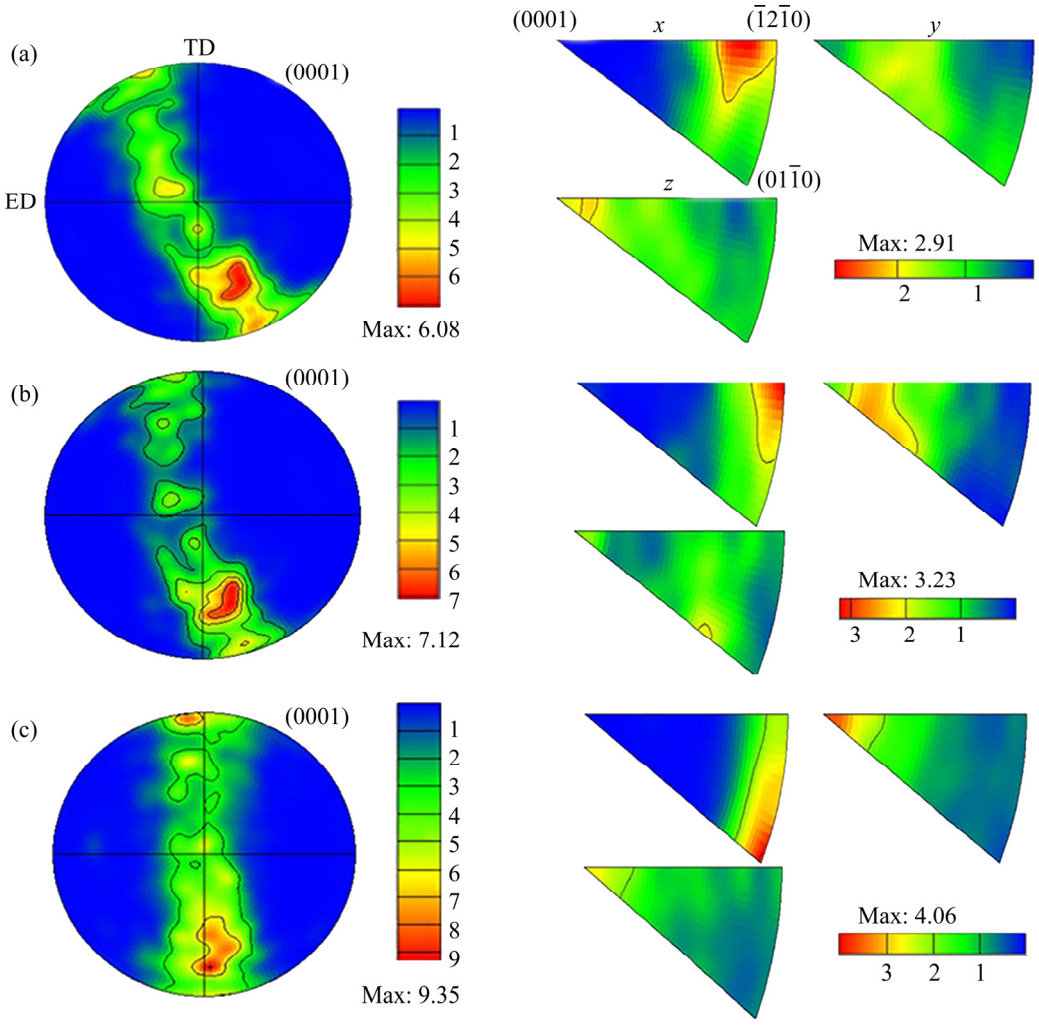

Fig. 11 Pole figures and inverse pole figures: (a) h=3 mm; (b) h=6 mm; (c) h=9 mm

pole densities of the pole figure are located at the bottom right of the center, which is related to the unique loading method of AFE. The pole figure is symmetrical in the center position, not by the TD or ED direction. When h=3, 6, and 9 mm, the pole densities are 6.08, 7.12, and 9.35, respectively. The weakening texture is more obvious when h=3 mm. The weakening texture is very beneficial to improving the ductility. However, most of the magnesium alloy produced by hot extrusion have a fiber texture (the C axis of the grain is parallel to the ND direction) [36]. In this work, the texture is significantly weakened at h=3 mm, because the DDRX has a weakening effect on the preferred orientation of grains. There is a certain misorientation between the grains and the parent grains, which has a certain weakening effect on the texture intensity [37].

When h=3 mm, a tilt angle of approximately 34° occurs. When h=6 mm, the tilt angle is reduced to approximately 10°. The appearance of the tilt angle is related to the grain rotation during the deformation process. As the loading displacement h of the split punch increases, the grains gradually move in the same direction from the original random disorder state.

In the inverse pole figure, only one texture component has a higher intensity at h=3 mm. There are multiple texture components when h=6 and 9 mm, which is mutually confirmed with the results obtained from the XRD.

In summary, texture intensity can be weakened by a small loading displacement, but the weakening effect is limited at large loading displacement.

4 Conclusions

(1) AFE is a new method for the refinement of grains. When the value of loading displacement (h) increases from 3 to 9 mm, the average grain size decreases from 14 to 9.5 μm. Moreover, The non-uniformity of grain size increases significantly, which can cause stress concentration and a decrease in the plasticity of the formed product.

(2) The tensile test results indicate that the UTS increases slightly with the increase in h values, but the elongation decreases significantly. Compared with h=9 mm, the elongation of the sample with h=3 mm reaches 29.41%, which is 3.33 times that of the former. The result suggests that texture weakening plays a significant role in the competition between grain boundary strengthening and texture weakening.

(3) With the decrease of h value in the AFE, the proportion of recrystallization gradually increases. Two main recrystallization mechanisms are DDRX and CDRX. As the value of h decreases from 9 to 3 mm, the texture intensity reduces from 9.35 to 6.08. The AFE undoubtedly provides a new idea and reference to improve the ductility of materials.

Acknowledgments

This work is supported by the National Natural Science Foundation of China (No. 51975166).

References

[1] SONG Jiang-feng, SHE Jia, CHEN Dao-lun, PAN Fu-sheng. Latest research advances on magnesium and magnesium alloys worldwide [J]. Journal of Magnesium and Alloys, 2020, 8(1): 1−41.

[2] WANG Yang, ZHANG Shun, WU Rui-zhi, TURAKHODIAEV N, HOU Le-gan, ZHANG Jing-hua, BETSOFEN S. Coarsening kinetics and strengthening mechanisms of core-shell nanoscale precipitates in Al−Li−Yb−Er−Sc−Zr alloy [J]. Journal of Materials Science & Technology, 2021, 61(2): 197−203.

[3] ZHAO Xi, LI Shu-chang, ZHENG Yang-sheng, LIU Zheng-ran, CHEN Kai, YU Jian-min, ZHANG Zhi-min, ZHENG Shun-qi. The microstructure evolution, texture weakening mechanism and mechanical properties of AZ80 Mg alloy processed by repetitive upsetting-extrusion with reduced deformation temperature [J]. Journal of Alloys and Compounds, 2021, 883: 160871.

[4] CHEN Gang, CHANG Xu-sheng, ZHANG Jing-xuan, JIN Yu, SUN Cheng, CHEN Qiang, ZHAO Zu-de. Microstructures and mechanical properties of in-situ Al3Ti/2024 aluminum matrix composites fabricated by ultrasonic treatment and subsequent squeeze casting [J]. Metals and Materials International, 2019, 26(10): 1574−1584.

[5] ZHAO Xi, YAN Fa-fa, ZHANG Zhi-min, GAO Peng-cheng, LI Shu-chang. Influence of heat treatment on precipitation behavior and mechanical properties of extruded AZ80 magnesium alloy [J]. Acta Metallurgica Sinica (English Letters), 2021, 34: 54−64.

[6] WANG Dan, LIU Shun-juan, WU Rui-zhi, ZHANG Shun, WANG Yang, WU Hua-jie, ZHANG Jing-huai, HOU Le-gan. Synergistically improved damping, elastic modulus and mechanical properties of rolled Mg−8Li−4Y−2Er−2Zn−0.6Zr alloy with twins and long-period stacking ordered phase [J]. Journal of Alloys and Compounds, 2021, 881: 160663.

[7] HUO Peng-da, LI Feng, WU Rui-zhi, GAO Rong-he, ZHANG An-xin. Annealing coordinates the deformation of shear band to improve the microstructure difference and

simultaneously promote the strength-plasticity of composite plate [J]. Materials & Design, 2022, 219: 110696.

[8] SIAHSARANI A, FARAJI G. Processing and characterization of AZ91 magnesium alloys via a novel severe plastic deformation method: Hydrostatic cyclic extrusion compression (HCEC) [J]. Transactions of Nonferrous Metals Society of China, 2021, 31(5): 1303−1321.

[9] AHMADI S, ALIMIRZALOO, FARAJI G, DONIAVI A. Properties inhomogeneity of AM60 magnesium alloy processed by cyclic extrusion compression angular pressing followed by extrusion [J]. Transactions of Nonferrous Metals Society of China, 2021, 31(3): 655−665.

[10] AYER O. A forming load analysis for extrusion process of AZ31 magnesium [J]. Transactions of Nonferrous Metals Society of China, 2019, 29(4): 741−753.

[11] FENG Jing-kai, ZHANG Ding-fei, HU Hong-jun, ZHAO Yang, CHEN Xia, JIANG Bin, PAN Fu-sheng. Improved microstructures of AZ31 magnesium alloy by semi-solid extrusion [J]. Materials Science and Engineering A, 2021, 800: 140204.

[12] PAN Fu-sheng, WANG Qing-hang, JIANG Bin, HE Jun-jie, CHAI Yan-fu, XU Jun. An effective approach called the composite extrusion to improve the mechanical properties of AZ31 magnesium alloy sheets [J]. Materials Science and Engineering A, 2016, 655: 339−345.

[13] YANG Qing-shan, JIANG Bin, ZHOU Guan-yu, DAI Jia-hong, PAN Fu-sheng. Influence of an asymmetric shear deformation on microstructure evolution and mechanical behavior of AZ31 magnesium alloy sheet [J]. Materials Science and Engineering A, 2014, 590: 440−447.

[14] ZHANG Wen-yan, ZHANG Hua, WANG Li-fei, FAN Jian-feng, LI Xia, ZHU Li-long, CHENG Shu-ying, ROVEN H J, ZHANG Shang-zhou. Microstructure evolution and mechanical properties of AZ31 magnesium alloy sheets prepared by low-speed extrusion with different temperature [J]. Crystals, 2020, 10(8): 644.

[15] ZHANG Ji-xiao, CHEN Liang, ZHAO Guo-qun, ZHANG Cun-sheng, ZHOU Ji-xue. Study on solid bonding behavior of AZ31 Mg alloy during porthole die extrusion process [J]. The International Journal of Advanced Manufacturing Technology, 2017, 93(5/6/7/8): 2791−2799.

[16] LI Feng, JIANG Hong-wei, LIU Yang. Microstructure and texture evolution during the alternate extrusion of an AZ31 magnesium alloy [J]. JOM, 2017, 69(1): 93−99.

[17] WANG Ye, LI Feng, WANG Yu, XIAO Xing-mao. Texture property and weakening mechanism of Mg−3Al−1Zn alloy by interactive alternating forward extrusion [J]. Journal of Magnesium and Alloys, 2021. DOI: 10.1016/j.jma.2021.05.007.

[18] WANG Yu, LI Feng, WANG Ye, GAO Lei. Effect of dynamic recrystallization on grain refinement during interactive alternating forward extrusion of AZ31B magnesium alloy [J]. Journal of Materials Engineering and Performance, 2020, 29(5): 2748−2756.

[19] GUO Kun-yu, XU Chang, LIN Xiao-ping, YE Jie, ZHANG Chong. Microstructure and strengthening mechanism of Mg−5.88Zn−0.53Cu−0.16Zr alloy solidified under high pressure [J]. Transactions of Nonferrous Metals Society of China, 2020, 30(1): 99−109.

[20] QIN De-hao, WANG Ming-jia, SUN Chao-yang, SU Ze-xing, QIAN Ling-yun. Interaction between texture evolution and dynamic recrystallization of extruded AZ80 magnesium alloy during hot deformation [J]. Materials Science and Engineering A, 2020, 788: 139537.

[21] GALIYEV A, KAIBYSHEV R, GOTTSTEIN G. Correlation of plastic deformation and dynamic recrystallization in magnesium alloy ZK60 [J]. Acta Materialia, 2001, 49: 1199−1207.

[22] PAEK S H, YU Hui,BAE J H, YIM C D, YOU B S. Microstructural evolution of indirect-extruded ZK60 alloy by adding Ce [J]. Journal of Alloys and Compounds, 2012, 545: 139−143.

[23] XU Yan, CHEN Chen, ZHANG Xu-xing, DAI Hao-hao, JIA Jia-bo, BAI Zhen-hua. Dynamic recrystallization kinetics and microstructure evolution of an AZ91D magnesium alloy during hot compression [J]. Materials Characterization, 2018, 145: 39−52.

[24] NIE Kai-bo, ZHU Zhi-hao, MUNROE P, DENG Kun-kun, GUO Ya-chao. Microstructure and mechanical properties of TiC nanoparticle-reinforced Mg−Zn−Ca matrix nano-composites processed by combining multidirectional forging and extrusion [J]. Transactions of Nonferrous Metals Society of China, 2020, 30(9): 2394−2412.

[25] JIANG Ju-fu, WANG Ying, LIU Ying-ze, XIAO Guan-fei, LI Hua. Microstructure and mechanical properties of 7005 aluminum alloy processed by one-pass equal channel reciprocating extrusion [J]. Transactions of Nonferrous Metals Society of China, 2021, 31(3): 609−625.

[26] HUANG K, LOGE R E. A review of dynamic recrystallization phenomena in metallic materials [J]. Materials & Design, 2016, 111: 548−574.

[27] Al-SAMMAN T, LI X, CHOWDHURY S G. Orientation dependent slip and twinning during compression and tension of strongly textured magnesium AZ31 alloy [J]. Materials Science and Engineering A, 2010, 527: 3450−3463.

[28] ZHAO Xi, LI Shu-chang, ZHANG Zhi-min, GAO Peng-cheng, KAN Shuai-ling, YAN Fa-fa. Comparisons of microstructure homogeneity, texture and mechanical properties of AZ80 magnesium alloy fabricated by annular channel angular extrusion and backward extrusion [J], Journal of Magnesium and Alloys, 2020, 8(3): 624−639.

[29] NAN Xiao-long, WANG Hui-yuan, ZHANG Lei, LI Jin-biao, JIANG Qi-chuan. Calculation of Schmid factors in magnesium: Analysis of deformation behaviors [J]. Scripta Materialia, 2012, 67(5): 443−446.

[30] WANG Ye, LI Feng, BIAN Nan, XIAO Xing-mao. Coordinated control of preferred orientation and uniformity of AZ31 in accumulative alternating back extrusion [J]. Materials Science and Engineering A, 2021, 818: 141366.

[31] XIN Re-long, WANG Mao-yin, HUANG Xiao-xu, GUO Chang-fa, LIU Qing. Observation and Schmid factor analysis of multiple twins in a warm-rolled Mg−3Al−1Zn alloy [J]. Materials Science and Engineering A, 2014, 596: 41−44.

[32] BARNETT M R. A Taylor model based description of the proof stress of magnesium AZ31 during hot working [J]. Metallurgical and Materials Transactions A, 2003, 34(9):

1799−1806.
[33] GUO Chang-fa, XIN Ren-long, DING Chang-hong, SONG Bao, LIU Qing. Understanding of variant selection and twin patterns in compressed Mg alloy sheets via combined analysis of Schmid factor and strain compatibility factor [J]. Materials Science and Engineering A, 2014, 609: 92−101.
[34] WANG Y, CHOO H. Influence of texture on Hall–Petch relationships in an Mg alloy [J]. Acta Materialia, 2014, 81: 83−97.
[35] ZHU S Q, YAN H G, LIAO X Z, MOODY S J, SHA J, WU Y Z, RINGER S P. Mechanisms for enhanced plasticity in magnesium alloys [J]. Acta Materialia, 2015, 82: 344−355.
[36] DU Yu-zhou, LIU Dong-jie, GE Yan-feng, JIANG Bai-ling. Effects of deformation parameters on microstructure and texture of Mg−Zn−Ce alloy [J]. Transactions of Nonferrous Metals Society of China, 2020, 30(10): 2658−2668.
[37] CAI Zhi-wei, CHEN Fu-xiao, MA Feng-jie, GUO Jun-qing. Dynamic recrystallization behavior and hot workability of AZ41M magnesium alloy during hot deformation [J]. Journal of Alloys and Compounds, 2016, 670(3): 55−63.

镁合金交互式交替正向挤压成形过程中显微组织演变及增塑机制

杜华秋[1]，李 峰[1,2]，霍鹏达[1]，王 宇[1]

1. 哈尔滨理工大学 材料科学与化学工程学院，哈尔滨 150040；
2. 哈尔滨理工大学 先进制造智能技术教育部重点实验室，哈尔滨 150080

摘 要：研究 AZ31 镁合金在不同加载位移(h=3、6、9 mm)下通过交互交替正向挤压方法加工的显微组织演变和力学性能。采用光学显微镜和电子背散射衍射分析显微组织演变，并通过拉伸实验与扫描电镜表征力学行为。结果表明，交互式交替正向挤压成形中连续动态再结晶(CDRX)与非连续动态再结晶(DDRX)共同作用实现晶粒细化。随着加载量 h 值的减小，再结晶占比由 23.4%提高到 66.7%。挤压丝织构逐渐向挤压方向(ED)倾斜，DDRX 的晶粒取向随机化效应进一步削弱纤维织构强度。当 h=3 mm 时，抗拉强度为 249.1 MPa，伸长率达到 29.4%。

关键词：镁合金；交替挤压；晶粒细化；织构弱化

(Edited by Bing YANG)